Construction and Building Materials 25 (2011) 2961–2971

Contents lists available at ScienceDirect

Construction and Building Materials

journal homepage: www.elsevier.com/locate/conbuildmat

Fracture mechanics of plate debonding: Validation against experiment

M. Achintha [a], C.J. Burgoyne [b,*]

[a] Solid Mechanics Group, Dept. of Engineering Sci., Univ. of Oxford, Parks Road, Oxford, OX1 3PJ, UK
[b] Dept. of Engineering, Univ. of Cambridge, Trumpington Street, Cambridge, CB2 1PZ, UK

ARTICLE INFO

Article history:
Received 3 December 2009
Accepted 18 November 2010
Available online 20 January 2011

Keywords:
Fracture energy
FRP (fibre reinforced polymers)
Energy release rate
Debonding
Critical crack length

ABSTRACT

The debonding of FRP plates from concrete beams is not amenable to finite-element analysis; fracture mechanics, based on a global energy balance, offers a better alternative. An analytical model with energy calculations based on a revised version of Branson's model (to take account of the reaction to the force in the FRP) has already been developed. This paper presents comparisons with a variety of experiments reported in the literature and shows that the model can correctly determine both the failure load and the failure mechanism. The paper shows that debonding often propagates in the concrete, just above the interface, and hence the failure load is dependent on the Mode I fracture energy of concrete. The method can also be used to determine when premature adhesive failure occurred prior to debonding within the concrete substrate.

1. Introduction

In an earlier paper [1], the authors have presented an analysis of the problem of premature debonding of FRP from concrete beams that relies on fracture mechanics and an assessment of the global energy balance. This paper provides experimental confirmation of the validity of that analysis by comparing the predictions with experiments carried out by others.

Premature plate debonding hampers efficient use of externally bonded FRP plates in flexural strengthening of concrete beams. Existing research mostly concentrates on finite element (FE) modelling of the concrete–FRP interface, but the sort of model that could be used in a FE analysis to follow the debonding-crack-tip behaviour requires far more detail than will ever be available to the designer or analyst, who would be forced to make unwarranted assumptions about interface properties [2]. Furthermore, the values returned by a FE program are governed by the smallness of the elements used: for example, there is an infinite stress concentration at the plate end which is detected when very fine meshes are used. None of the existing models have received wide acceptance and most have only been calibrated against each researchers' own set of test data, which is usually limited in extent.

The concepts that underlie fracture mechanics better simulate failures taking place at interfaces of dissimilar materials and have been used effectively in interface debonding studies in thin-layered elastic materials (e.g. [3]). There has been some recent work that applied fracture-mechanics concepts to FRP debonding from concrete, but these have directly used linear-elastic-fracture-mechanics (LEFM) concepts as applied to the analysis of thin-layered elastic materials (e.g. [4]). A reliable FE analysis to determine the crack-tip stress field in concrete cannot be obtained because of the unknowable microstructure. In addition, the assumptions on which the LEFM is based are not justified for concrete because of the large fracture process zone [2].

The present fracture mechanics model assumes that flaws are inevitable in the interface and investigates how the global energy balance of the beam changes during a small potential crack extension; an existing crack *will* propagate if the energy release rate (i.e. energy available for crack to propagate – G_R) exceeds the interface fracture energy (i.e. the energy needed to form the required new surfaces – G_F). The energy evaluation of the beam is based on a revised version of Branson's model which determines the moment–curvature behaviour of a cracked beam, subject to an external compressive force (the reaction to the tension force in the FRP); this analysis is described elsewhere [1,5]. Debonding will propagate in whichever of the concrete, adhesive, or an interface (concrete–adhesive or adhesive–FRP) that provides the least resistance; G_F is thus the fracture energy of that weakest phase. Determination of G_F is not trivial; however, justifiable estimations, within the accuracy expected in the analysis of concrete beams, can be made. That work is briefly reviewed below but described in a separate publication [6].

The plate end, where abrupt curtailment of the plate causes a change in geometry and where there is also a variation in strength, is one of the areas most susceptible to the initiation of debonding. Others are the locations where the widening of flexural and/or

* Corresponding author. Tel.: +44 1223 332698; fax: +44 1223 332662.
E-mail addresses: engs0820@herald.ox.ac.uk (M. Achintha), cjb@eng.cam.ac.uk (C.J. Burgoyne).

0950-0618/$ - see front matter © 2010 Elsevier Ltd. All rights reserved.
doi:10.1016/j.conbuildmat.2010.11.103

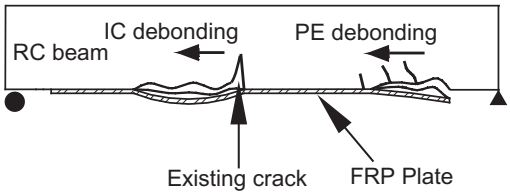

Fig. 1. Two modes of debonding.

flexural-shear cracks cause interface cracks; the two modes are referred to as "plate-end (PE) debonding" and "intermediate-crack-induced (IC) debonding" respectively (Fig. 1); the model analyses both modes. Despite the crack-tip stress field not being amenable to precise analysis, the energy level of the whole beam can still be calculated to a reasonable accuracy because the Branson's model represents the average moment–curvature (and hence the energy levels) of beam cross sections distributing all complex stress conditions that will be present in beam sections. The unreliable stress predictions in the crack-tip vicinity are therefore not critically significant to the energy balance of the whole system, whereas the crack-tip stress field would solely govern an analysis based on LEFM [1].

2. Critical crack concept for the debonding analysis

The model is intended to determine "*the longest interface crack that can be sustained without causing debonding under a given applied load*", or alternatively, "*for a given crack geometry what is the maximum load that can be sustained?*".

Despite numerous cracks inevitably being present in the interface, usually none is long enough nor weak enough to cause failure by itself. Nevertheless, they can coalesce by growing slowly, and subsequently form a longer crack that can propagate steadily, ultimately causing separation of FRP from the concrete beam. Determination of the failure load and the debonding mode are the objectives of this study, so the analysis is based on the steady propagation of the dominant crack that will eventually trigger the ultimate failure [1]. Neither the development of microcracks nor the slow growth of macrocracks is generally amenable to analysis, so the model adopted here is based on steady propagation of the dominant crack as has been done in pioneering linear-elastic fracture analyses (e.g. [3]).

The present model defines the *critical crack* as the smallest crack that can propagate steadily under the given conditions. This concept is very useful in concrete where significant microcracking is inevitable prior to the formation of the critical crack. As is shown below, the critical crack concept adopted in the analysis correlates well with test data.

3. Interface fracture energy

A critical parameter in the present analysis is the magnitude of the interface fracture energy (G_F), but despite considerable research, none of the existing studies provides a reliable estimate. There exist many conceptual misunderstandings; for example, failure phase, fracture mode, size effects of concrete etc. have not been properly taken into account. A wide range of arbitrary values have been selected that correlate well with results from individual test programmes.

Experimental observations confirm that the concrete substrate just above the interface is the most likely place for failure to occur, especially when the adhesives recommended by the FRP manufacturer are used with appropriate curing procedures. Despite the inevitable presence of both shear and peeling stresses at the crack tip, shear tractions of concrete can only realistically occur with

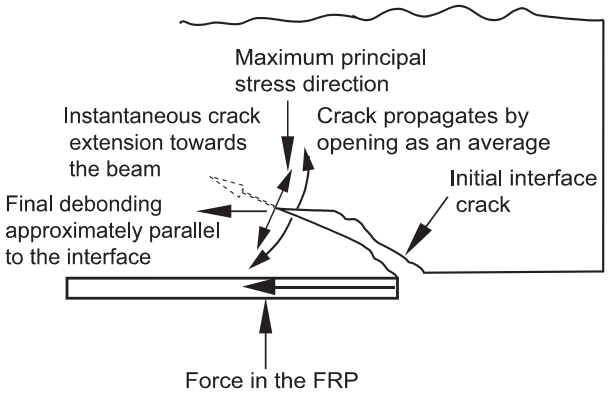

Fig. 2. Debonding propagates in Mode I as an average.

large crack-plane separations [6]. Hence the shear-mode fracture energy is not a factor in plate debonding where a narrow crack opening triggers the instantaneous crack extension. It is contended that an interface, which is primarily carrying shear, actually fails in tension. Since principal stress would be at about 45° to the interface, any crack would move into the beam (Fig. 2); however, this will not happen since the FRP force acts eccentrically to the tip of the crack, causing a moment that causes tension in the tip, which then moves back down towards the interface (Fig. 2). The present analysis avoids a detailed study of the crack-tip stress field, but assumes that extension of debonding is a Mode I propagation as an average, even if the local details may not be Mode I governed. The relevant G_F is thus the same as the "opening mode" (Mode I) fracture energy of concrete (G_{Cl}); comparisons with test data validate the assumption (detailed analysis of the fracture energy of the concrete–FRP interface is described in a separate publication [6]).

3.1. Adhesive failure

The recommendations of the FRP manufacturer on selection and curing of adhesives, together with the existing knowledge on application of external FRPs on concrete surfaces, usually means that premature adhesive failure can be avoided. However, use of a weak adhesive or poor workmanship can trigger premature adhesive failures prior to the expected debonding within the concrete substrate.

Determination of the fracture energy of adhesive is not trivial and the fracture properties are influenced by many factors such as the chemical composition, curing method, temperature and moisture content; most of these effects cannot be known with certainty and may be commercially confidential (e.g. [7]). No estimates are made for the fracture energy of adhesive in this study; nevertheless, the known concrete fracture energy can be used to distinguish when premature adhesive failure occurred (an example is discussed in Section 6.4 below).

4. Identification of critical parameters

Plate end (PE) debonding propagates into the beam whereas intermediate-crack-induced (IC) debonding propagates towards the nearest beam end (Fig. 1). The plate end location is most influential on PE debonding whereas the interface crack length and its location within the beam govern IC debonding [1].

4.1. Plate-end debonding

Plate-end debonding initiates from a shear crack that develops at the plate end and propagates in the beam towards the internal tension steel (Fig. 3a) (e.g. [8,9]). This shear crack causes partial

separation of the FRP from the concrete beam resulting in an interface crack. The peeled part of the plate carries no force, so the effective plate end location (L_{0_eff}) is now placed slightly away from the actual plate end. How far the initial shear crack develops prior to the attainment of the critical debonding state determines the location of L_{0_eff}, which in turn governs the associated energy release rate (G_R). The method for calculating G_R for a given plate-end location has been presented elsewhere [1]. If the associated G_R is sufficient to cause debonding then the propagation will start before the initial crack reaches the tension steel. It is assumed that the initial shear crack propagates at about 45° to the beam axis (e.g. [8,9]); thus, the additional ineffective length of the FRP just before critical debonding is expected to be within one cover distance (c) from the actual plate end.

When the G_R associated with the original interface crack created by the shear crack at the plate end is not sufficient to cause debonding, the crack may extend slowly in an approximately horizontal direction at the level of the tension steel (e.g. [10]) (Fig. 3b). This slow crack growth will continue until the associated G_R reaches G_{Cl} and thereafter critical debonding will propagate. Knowledge of the location of the tip of the interface crack just prior to reaching the critical debonding state (i.e. L_{0_eff}) is a prerequisite in the analysis.

If the interface cracks that develop in the plate-end vicinity are incapable of triggering PE debonding (i.e. when the associated $G_R \ll G_{Cl}$), it is possible to initiate debonding by the widening of a shear crack some distance away from the plate end (e.g. [11]) (Fig. 3c). This mode of debonding is expected when the FRP is extended close to the beam support. Widening of shear cracks produces high stress concentrations and the subsequent diagonal microcracks can cause the separation of that narrow portion of the FRP towards the plate end (Fig. 3c). The plate is now effective at the bottom of the critical shear crack, a relatively high moment zone – i.e. the energy changes associated with a small crack extension will be significant, and the consequently higher G_R values may trigger debonding. The location of the critical shear crack needs to be taken as the effective plate end location (L_{0_eff}) in the analysis (Fig. 3c).

4.2. Intermediate-crack-induced debonding

While the effective plate end location (L_{0_eff}) governs PE debonding, the analysis of IC debonding is more complicated since the partly-debonded plate is still attached to the concrete beam at both ends of the debonded zone, and must also satisfy compatibility of extension with the concrete beam [1]. It has been shown that, in simply-supported beams, IC debonding initiates in the high moment zone and propagates towards the beam support, validating the experimental observations [1]. The analysis has also shown that the *length* of the existing debonding crack must be investigated, together with its *location* in the beam, but both are rarely available even in a closely monitored test programme because the sudden nature of debonding makes the identification of the critical flaw extremely difficult [2]. Most existing analyses have assumed that IC debonding is triggered by high interfacial stresses caused by the sudden increase in stress transfer from the concrete beam to the FRP at a crack location. However, the exact crack geometry and also the effects of the relative sliding/rotation of the two crack faces are unknown; the existing analyses have not been correlated well with test data.

The present model investigates the possible propagation of an existing crack and it is not possible, or necessary, to say what caused the original interface flaw. It is sufficient to say that flaws of the relevant size are *likely* to exist in a critical location. Thus, the model has to identify the length of the critical crack that triggers debonding at a given location or the failure load for a given crack length and location.

It is contended that, in simply-supported beams, IC debonding might start near the mid-span of the beam since it requires the development of much shorter interface cracks [1]. As was noted in some of the test programmes (e.g. [12]), widening of flexural cracks in the high moment zone can cause interface cracks long enough to trigger debonding (Fig. 4a). However, in shear-dominant beams (i.e. beams with smaller shear-span to beam-depth ratios) widening of flexural cracks might not develop interface flaws that are long enough to trigger IC debonding. Nevertheless, widening of flexural/shear cracks will cause much longer interface flaws here because of the considerable vertical relative sliding between the two crack surfaces. Therefore, debonding can initiate some distance away from the high moment zone (see Fig. 4b). Despite exact analytical predictions not being available for the critical crack locations and lengths, justifiable assumptions can be made, as is shown below.

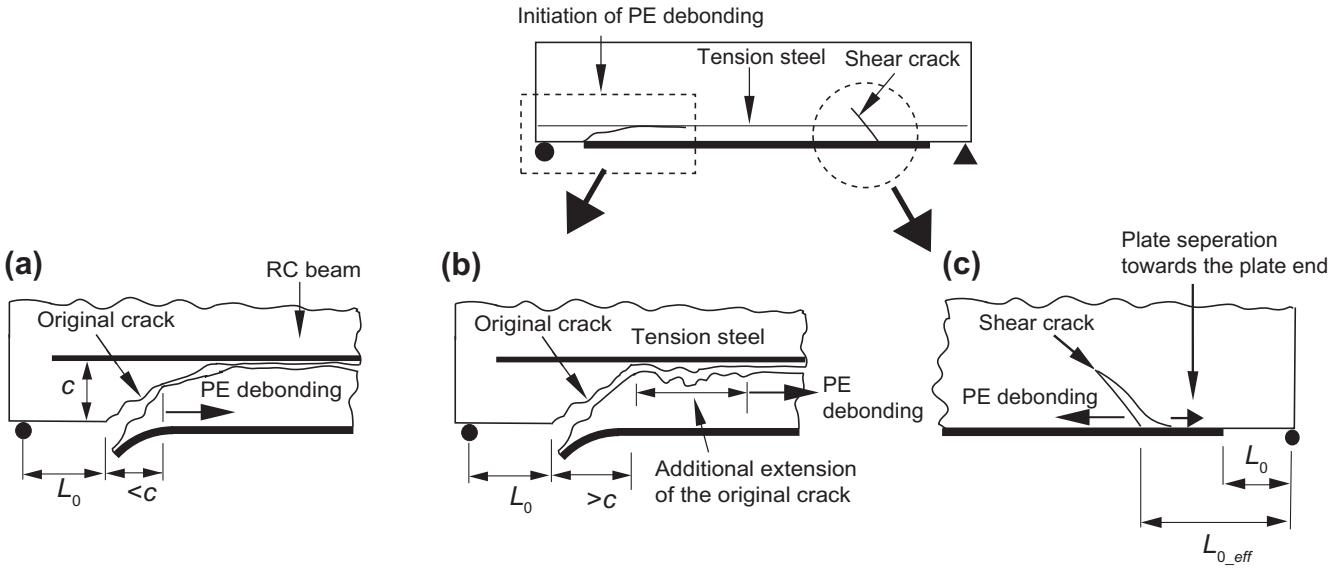

Fig. 3. Initiation of PE debonding. (a) Before the original crack reaches the steel bars, (b) after further slow horizontal crack extension at the steel bar level and (c) by widening of a shear crack in the span.

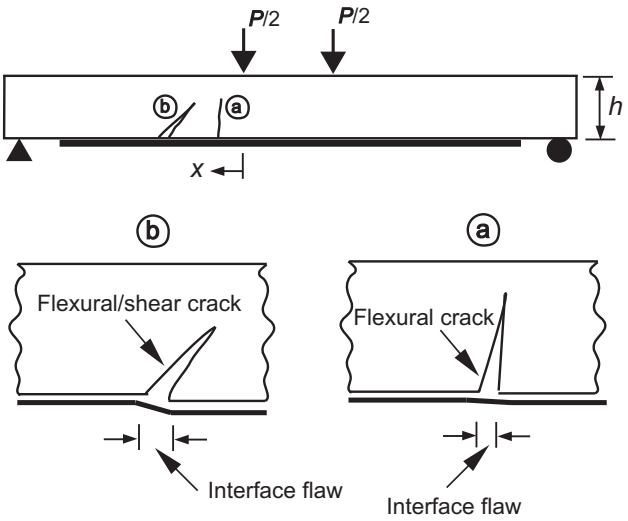

Fig. 4. Initiation of IC debonding: by widening of (a) flexural crack (b) flexural/shear crack.

5. Comparisons with tests: overview

The model has been validated against a database of test results, collected from the literature, covering all possible forms of PE and IC debonding. Due to space constraints, only a limited number of such comparisons are shown here, but they have been selected to cover test specimens with a large variety of material and geometric properties. It is also shown that the model can also be used for debonding analysis of beams strengthened with steel plates, when the steel plates remain within elastic limits.

All the beams analysed here were tested as simply-supported beams under four-point bending with equal shear spans (Fig. 5). The material and geometric properties of the specimens are given in Table 1. Assumed values have been used for any missing data in the original publications: normally only the thickness and the shear modulus of the adhesive are absent in the original publications, which are less significant for the current analysis unless a particular case of premature adhesive failure is being studied. When details of the aggregate were not quoted, properties have been assumed such that the results from the analysis are consistent with all the test data reported from that study. When available, load–deflection curves of both strengthened and control (i.e. unstrengthened) beams were validated prior to the debonding analysis.

5.1. Failure load and fracture energy for comparisons

For each chosen example, the energy release rate (G_R) corresponding to an assumed debonding crack at the reported failure load ($P_{failure}$) is compared with the Mode I fracture energy of concrete (G_{Cl}). However, there is uncertainty of all the parameters, so to illustrate the significance of the variability, the results for a ±10% variation in $P_{failure}$ and a ±10% variation in G_{Cl} are considered.

5.2. Mode I fracture energy of concrete

LEFM cannot be used to determine G_{Cl} because of the long fracture process zone associated with concrete fracture. It is contended that Hillerborg's cohesive-crack-model-based experimental and approximate theoretical models better estimate G_{Cl} [2]. G_{Cl} of concrete depends on the aggregate size and type (i.e. surface texture), and strength (i.e. the water/cement ratio) and can be determined to sufficient accuracy from standard fracture tests (e.g. [13]), which are now well established. In addition, approximate tension-softening models, presented in terms of more readily known properties of concrete (e.g. tensile strength and the maximum aggregate size) can also be used to determine G_{Cl} of a given mix.

All but one set of beams discussed in this paper were tested with normal strength concrete (30–55 N/mm^2) where G_{Cl} is expected to depend on the size and the surface texture of aggregates. 20 mm and 10 mm crushed aggregates and rounded aggregate (i.e. river gravel) of 10 mm were used in the test beams. The test data reported in the literature quoted a value about 0.15 N/mm for concrete with 20 mm crushed aggregate and whereas those with 10 mm crushed and rounded aggregates were reported to be about 0.10 and 0.07 N/mm respectively (e.g. [14]). These values correlate well with the predictions from the tension-softening models and also with a widely verified empirical model (this study is described elsewhere – [6]); the quoted values are used in the comparisons shown below.

6. Comparisons with experimental results: plate-end debonding

6.1. Examples: plate-end debonding initiating in the actual plate-end vicinity

The variation between the actual plate end (L_0) and predicted effective plate end location (L_{0_eff}) is expressed in terms of the depth of the cover (c): results are normally fitted between $L_0 - 2c$ and $L_0 + 2c$. The best possible agreement between theory and test would be for failure at $P = P_{failure}$; $G_R = G_{Cl}$ to occur at the observed L_{0_eff}.

6.1.1. Fanning and Kelly [9]

Fanning and Kelly [9] tested four beam pairs, identical apart from having different lengths of external CFRP plates. Two of these pairs failed in PE debonding with consistent failure loads; debonding in those beams (quoted in Table 1) were analysed in the present study. The average value of the two failure loads was used in

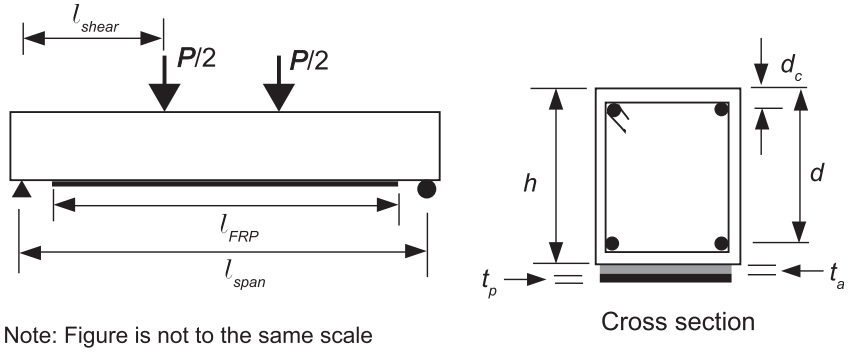

Fig. 5. Geometric and loading data for four-point bending.

Table 1
Identification, geometric and material data of the beams used in the plate-end debonding analysis.

Reference	Beam specimen	Failure load (kN)	Plate material	l_{span} (mm)	l_{shear} (mm)	Aggregate (type/size)	L_0	b	h	d	d_c	A_{st}	A_{sc}	c	f'_c	f_{y_s}	f_{y_sp}	t_p	A_p	E_p	t_a	G_a
Fanning and Kelly [9]	F3 & F4	101.5	CFRP	2800	1100	20 (crushed)*	385	155	240	203	37	339	226	31	80	530	530	1.2	144	155	3.0	6.0*
	F9 & F10	72.0					550															
Arduini et al. [8]	A4	110.0	CFRP	2000	700	10 (rounded)*	150	200	200	163	37	308	308	30	31	540	540	1.3	195	167	2.0*	11.0
	A5	86.0																	390 (2 layers)			
Nguyen et al. [10]	A950	56.2	CFRP	1330	440	20 (crushed)*	190	120	150	120	25	236	56.5	25	32.1	384	400	1.2	96	181	1.5	12.8
	B2	130					115					628		20	44.6	466						
Triantafillou and Plevris [15]	B8	37.4	CFRP	1220	458	10 (crushed)	75	76	127	111	16	33.2	33.2	14	44.7	517	517	1.9	120	186	2.0*	6.0*
Mohamed Ali et al. [11]	SP-T 6	112.5	Steel	4700	1250	10 (crushed)	50	200	370	330	35	1257	157	30	35	530*	530*	6	1200	200	2.0*	6.0*
Quantrill et al. [16]	B2	34.0	GFRP	1000	300	10 (rounded)	20	100	100	69	31	84.8	56.5	20	42	400	400	1.2	96	49	2.0*	11.0*
	B3	12.3																	36			
Ross et al. [17]	Group 1	101.5	CFRP	2742	914	10 (crushed)	N/A	200	200	152	20	141.8	141.8	20	54.8	540	540	0.45	90	138	2.0*	4.8*
	Group 2	72.0										257.4										
	Group 3	116										402.1										
Garden et al. [12]	$3_{U,1.0}$	34.0	CFRP	1000	340	10 (crushed)	N/A	100	100	84	16	84.8	56.5	10	46	350	350	0.82	55.0	111	2.0	8.6

Note: The length, area, strength, stiffness quantities have units mm, mm^2, N/mm^2 and kN/mm^2 respectively.
* Indicates assumed values.

the comparisons. Fig. 6 shows the variation in G_R against L_{0_eff} of two selected beam pairs. The aggregate type used in the mix was not quoted, but for both beam pairs the observed failure loads agree well with G_{Cl} about 0.15 N/mm, which is the value usually expected for a concrete with 20 mm crushed aggregate. Fig. 6 shows that taking L_{0_eff} of 6.5 and 10 mm higher than the actual L_0 (the cover is 30 mm) predicts the reported debonding loads of the two beam pairs. The same figures also show that at the observed failure loads any L_{0_eff} shorter than the actual L_0 could not cause PE debonding: a real interface crack (i.e. with a positive magnitude) is required to trigger debonding.

Fig. 6 also shows the predicted L_{0_eff} if failure had occurred at loads 10% higher or lower load than the observed failure load. For both beam pairs these two load levels are too strong or too weak respectively to cause PE debonding within the range between L_0 and $L_0 + c$; the theory thus matches the observed failure load and failure mode.

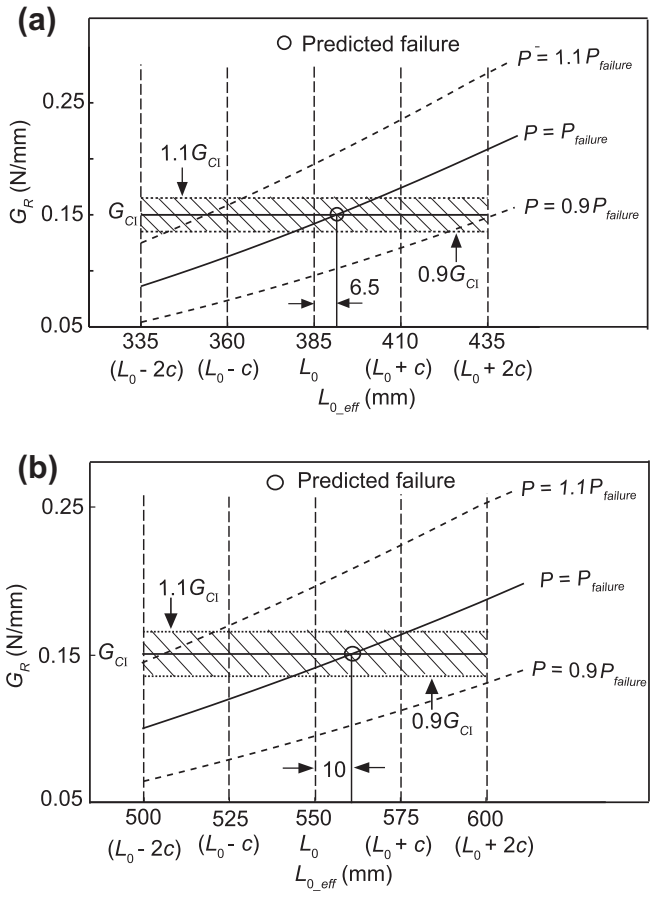

Fig. 6. G_R vs. L_{0_eff} plots for (a) F5 and F6. (b) F9 and F10 (Fanning and Kelly [9]).

6.1.2. Triantafillou and Plevris [15]

Triantafillou and Plevris [15] investigated the effect of the CFRP plate area on the failure load and the failure mode of strengthened beams. The beam strengthened with the thickest plate (1.9 mm), Beam No. 8 of their test programme (quoted in Table 1), failed by PE debonding that initiated at the plate end; the failure of that beam is studied. 10 mm crushed aggregate was used in the test programme, so G_{Cl} is assumed to be 0.1 N/mm. The G_R vs. L_{0_eff} plot shown in Fig. 7 predicts that the critical interface crack would be about 2 mm long, which correlates well with the reported failure

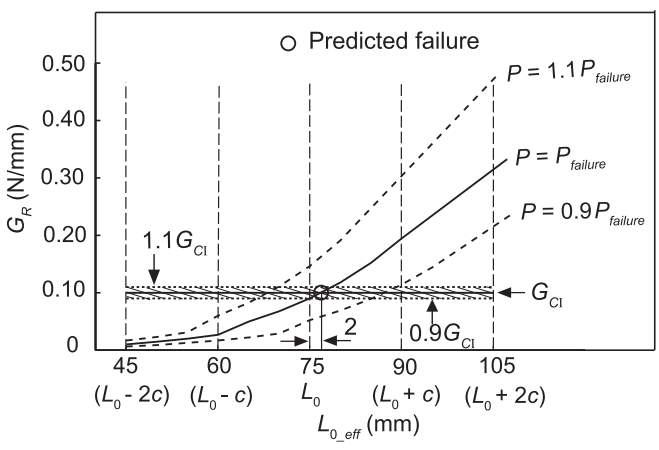

Fig. 7. G_R vs. L_{0_eff} plot for Beam 8 (Triantafillou and Plevris [15]).

mode: sudden debonding immediately after the formation of the plate-end shear crack. The same figure also shows that neither a load 10% higher nor lower than the actual failure load would cause the observed sudden failure.

6.1.3. Arduini et al. [8]

Fig. 8 shows G_R vs. L_{0_eff} plots for two beams, A4 and A5, tested by Arduini et al. [8] Beam A4 was strengthened with a single layer of CFRP plate (curtailed at L_0 = 150 mm), and failed by PE debonding at the internal tension steel level which originated as a shear crack at the plate end. So it is expected that the L_{0_eff} for this case should be about 180 mm as the cover to the main steel bars is 30 mm. Fig. 8a shows that a L_{0_eff} of 175 mm would give the observed failure load if G_{Cl} was 0.07 N/mm. The aggregate type was not quoted, but G_{Cl} of a normal strength concrete mix with 10 mm rounded aggregate is about 0.07 N/mm, so it is assumed that 10 mm rounded aggregate was used in the tests, which would be reasonable given the small size of the beams (Table 1). The same figure also shows that neither an L_{0_eff} less than the actual L_0, nor a load lower than 90% of the reported failure load would cause PE debonding. A 10% higher load however can cause the failure within the expected L_{0_eff} range but only requires a critical interface crack about 6 mm long. This however does not agree with the observed failure mechanism in which the shear crack develops up to the tension steel level prior to sudden debonding.

Beam A5 was identical to Beam A4 except that it was strengthened with two layers of CFRP. Fig. 8b shows the G_R variation for Beam A5 at the reported failure load level within the assumed

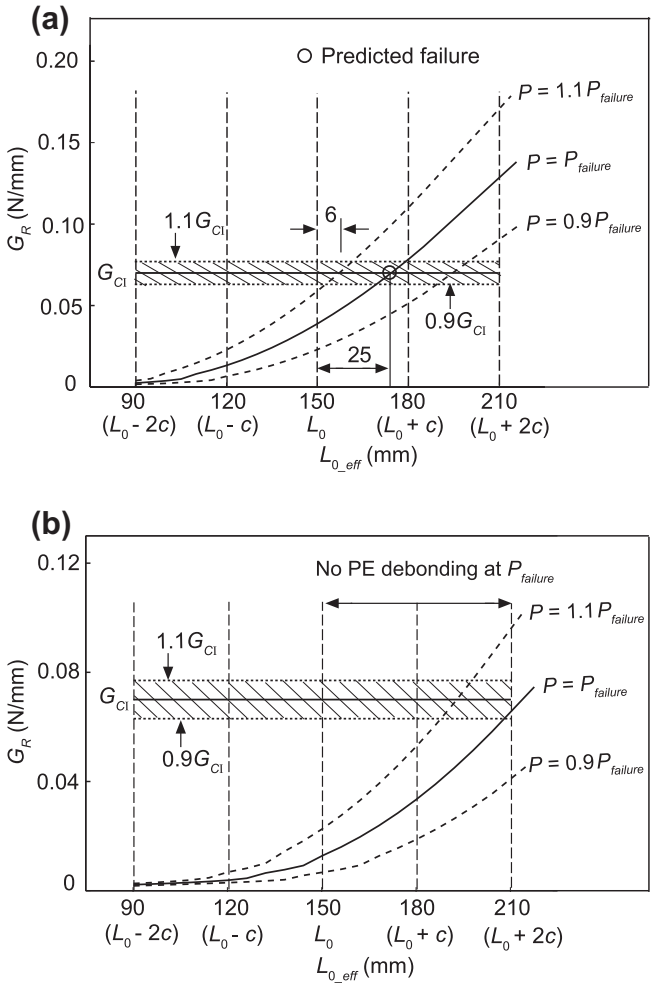

Fig. 8. G_R vs. L_{0_eff} plots for beams. (a) A4 (b) A5 (Arduini et al. [8]).

L_{0_eff} range. The minor unevenness in the G_R plot is due to the change in the cracking state of the transfer zone sections (where force in the FRP is building up to its fully-bonded value) from being uncracked to partially-cracked; as not all the sections in this critical zone change their cracking state at the same time, a small waviness in the G_R plot occurs [1]. The figure shows G_R values smaller than the assumed G_{Cl} (0.07 N/mm) for $L_{0\_eff} < L_0 + 2c$ and hence indicates that a critical debonding crack could not develop in the vicinity of the plate end. In fact, a shear failure was reported for this beam. The formation of more significant stress concentrations in the plate-end vicinity because the two layers of CFRP plates are stiffer could have led to this premature shear failure. This problem, however, is beyond the scope of the present study.

6.2. Example: debonding after additional horizontal propagation of the plate end crack

Two similar beams tested in Nguyen et al. [10], Beams A950 and B2, with different internal tension steel arrangements, were strengthened with CFRP plates of different lengths (quoted in Table 1); both beams failed due to PE debonding. However Beam A950, which was strengthened with the much shorter CFRP, failed immediately after the formation of the plate-end shear crack (i.e. the failure mechanism shown in Fig. 3a) whereas Beam B2 showed an additional resistance even after the shear crack extended up to the internal steel bars (i.e. the failure mechanism shown in Fig. 3b). The aggregate type used in the mix was not quoted, but as shown in Fig. 9 for both pairs of beams the observed failure loads agree well with G_{Cl} of 0.15 N/mm, which corresponds to a concrete with 20 mm crushed aggregate.

The G_R vs. L_{0_eff} plot of Beam A950 (Fig. 9a) shows that any infinitesimal crack would cause PE debonding at $P_{failure}$. The same figure also shows that a much longer crack would have propagated at a lower load (for example, an interface crack about 20 mm would propagate at 90% of the observed failure load). But that would have required the development of the subcritical crack up to this critical length and hence the beam should have resisted additional load after the formation of the critical shear crack. However, the beam failed suddenly with the formation of the shear crack at the plate end, which matches the prediction of the present analysis.

The G_R vs. L_{0_eff} plot for Beam B2 (Fig. 9b) shows that the interface crack needed to develop for an additional distance about 18 mm after reaching the level of the tension steel bars to cause debonding, which matches the reported additional load resistance of the beam after the formation of the interface crack. The actual location which the critical crack reached was not quoted, so further comparisons cannot be made.

6.3. Examples: plate-end debonding initiating from intermediate shear cracks

This mode of PE debonding has been observed when the external plate extends towards the beam support, in particular, in steel-plate-bonded beams. Although developed for use with FRP, the present model should be applicable to steel plates which remain within elastic limits. Beam SP-T 6 tested in Mohamed Ali et al. [11] was strengthened with a steel plate curtailed 50 mm from the beam support, but PE debonding initiated by widening of a shear crack located at 300 mm away from the plate end. The concrete used had 10 mm crushed aggregate so the G_{Cl} is assumed to be 0.1 N/mm. The G_R values corresponding to the actual plate-end vicinity confirm that a critical interface crack in the region could not develop in that region (Fig. 10). But, the figure shows that G_R associated with L_{0_eff} of about 350 mm (i.e. at the noted critical shear crack location – L_{0_crack}) causes PE debonding at the reported failure load.

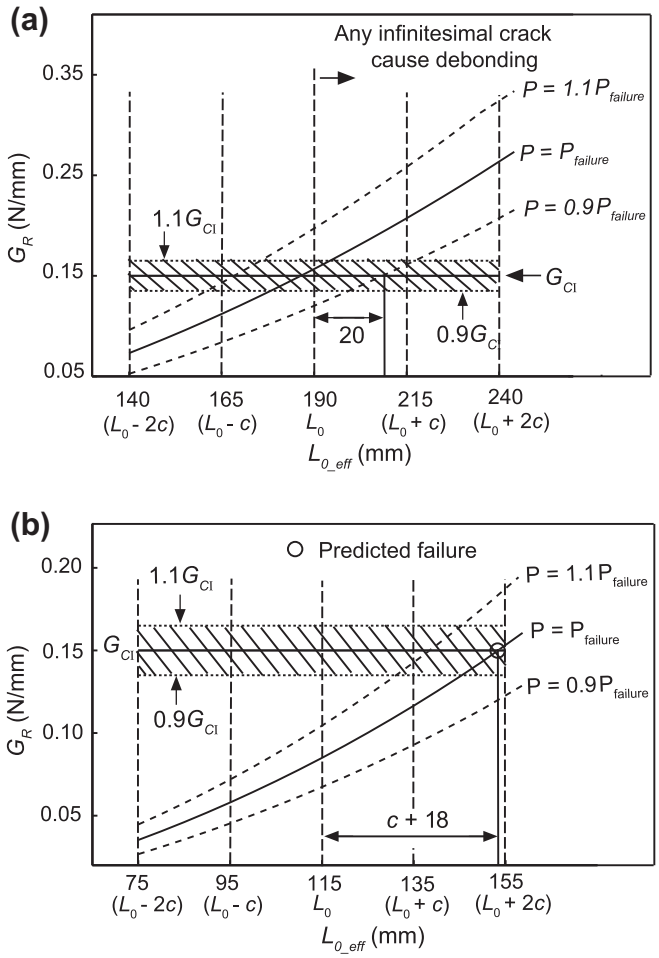

Fig. 9. G_R vs. L_{0_eff} plots for beams. (a) A950 (b) B2 (Nguyen et al. [10]).

6.4. Examples: plate-end debonding propagating within the adhesive layer

Beams B2 and B3 tested by Quantrill et al. [16] failed by PE debonding, with L_{0_eff} in the range 20–80 mm [2]. Interface concrete failure was reported for B2 whereas B3 failed by premature debonding in the adhesive layer. Ten millimeter rounded aggregate was used in the test programme, so, G_{Cl} is assumed to be 0.07 N/mm. Fig. 11a shows G_R vs. L_{0_eff} plot at the reported failure load of B2; the figure justifies the observed interface-concrete debonding at the reported failure load. The G_R vs. L_{0_eff} plot for B3 (Fig. 11b) shows that the associated G_R values are less than about 50% of G_{Cl} and hence a failure of concrete in the vicinity of the interface is less likely to happen at the reported failure load. It is assumed that the adhesive must have had a fracture energy less than 0.04 N/mm.

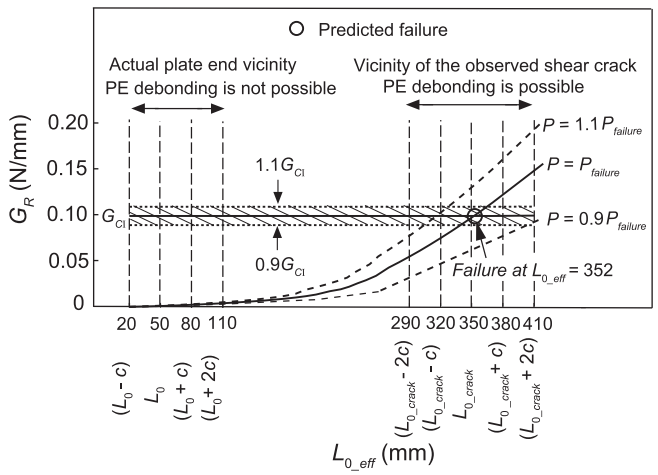

Fig. 10. G_R vs. L_{0_eff} plots for beam SP-T 6 (Mohamed Ali et al. [11]).

7. Comparisons with experimental results: intermediate-crack-induced debonding

IC debonding is more complex than PE debonding since the *likely length* of the existing debonding crack must be investigated together with its *location* in the beam. Neither parameter can be known precisely; justifiable assumptions can however be made.

As is shown below, most beams failed due to propagation of cracks 2–3 mm long, caused by the widening of flexural cracks, whereas in much shorter beams, longer interface flaws, about 5 mm long that result from the widening of flexural/shear cracks, initiated the failure. The exact location of the critical flexural crack cannot be known, but the results show that, for four-point bending, the assumption that IC debonding initiates from a location half a beam depth away from the loading point towards the support gives accurate comparisons with test data. This agrees with direct test observations (e.g. [12]) and makes sense since the failure initiates in a region with both high moment and high shear.

7.1. Examples: IC debonding initiated by widening of flexural cracks

The observed IC debonding failures of three sets of beams (Groups 1–3) reported in [17] are analysed, assuming that debonding initiates by widening of a flexural crack in one of the shear spans at a half beam depth (h) away from the loading point.

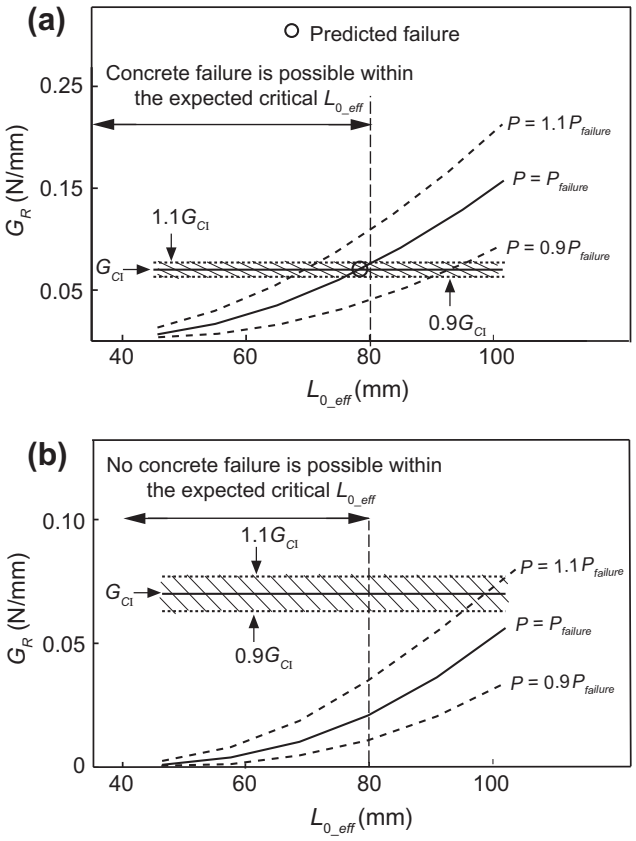

Fig. 11. G_R vs. L_{0_eff} plots for beams. (a) B2 (b) B3 (Quantrill et al. [16]).

Possible crack-origin locations, a further half and a full beam depth towards the nearest beam end are also investigated. The stress distribution very close to the loading point will be of a very complex nature and could not be analysed using the section analysis adopted here, and hence the possibility of debonding initiating much closer to the loading point is not investigated. As IC debonding usually takes place at higher applied load levels (often above 90% of the expected ultimate failure load) only the possibility of debonding propagation at a 10% lower load than the reported failure load ($P_{failure}$) is investigated.

The solid line in Fig. 12a shows the variation in G_R against l_d (crack length) of a Group 1 beam for an interface crack that initiated at the assumed critical location ($x_{critical}$) at $P_{failure}$. G_{Cl} is assumed to be 0.10 N/mm for the used mix with 10 mm crushed aggregate. The figure shows that l_d of 2 mm would cause debonding here. As noted in [12], the widening of a critical flexural crack in the high moment zone causes interface flaws of this magnitude.

The same figure (dashed lines in Fig. 12a) also shows that much longer critical cracks of lengths 3.5 and 6 mm must be developed to cause debonding at $P_{failure}$ if the debonding initiates at a half and a full beam depth away towards the nearest beam end, which are less likely to occur. The possibility that debonding initiates at the assumed critical location at 90% of $P_{failure}$ is investigated in Fig. 12b. The figure shows that the critical l_d (l_{d_cr}) here needs to be about twice that required at $P_{failure}$, so is less likely.

The analysis of the other two groups of beams (Groups 2 and 3) gave similar results. Table 2 compares the calculated l_{d_cr} for groups of beams (beams are identical except for the amount of internal tension steel). The table shows that debonding cracks about 2–3 mm long that start at a half beam depth away from the loading point would cause failure in all three beam groups.

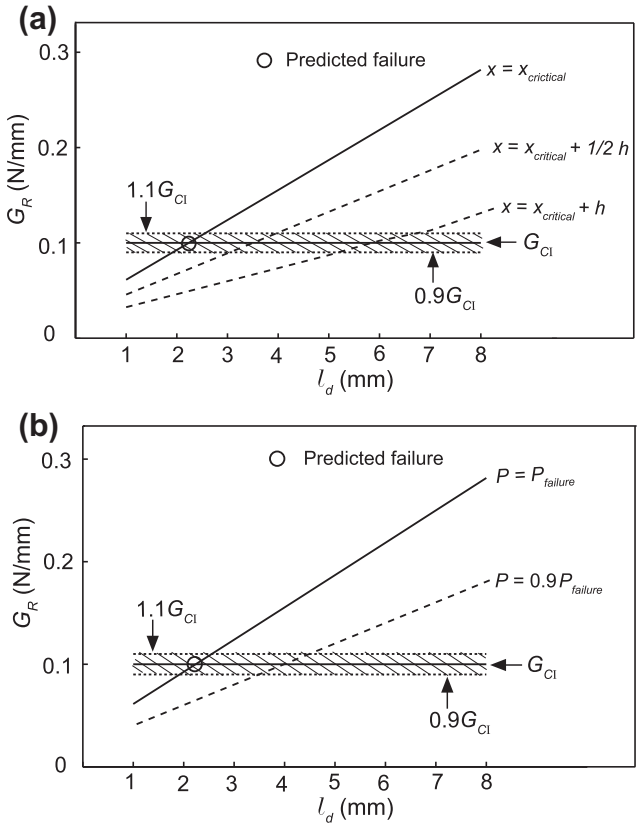

Fig. 12. G_R vs. $l_{d\ plot}$ for Group 1 beam (Ross et al. [17]) for fractures starting at (a) different locations (b) 90% of the failure load.

Table 2 also shows that much longer cracks, often longer than twice l_{d_cr}, would be needed if the crack developed further a half and a full beam depth away towards the nearest beam end, so it is much less likely that failures would occur. The Group 1 beam was lightly reinforced whereas the Group 3 beam had more steel, so would have had less flexural cracking. This is shown by the significant increase in l_{d_cr} as the crack location moves away from the high moment zone. Table 2 further shows that, for all three beam groups, much longer interface cracks than would normally be caused by widening of flexural cracks are required to cause debonding at 90% of the respective reported failure loads.

The reported failure loads of the Groups 1–3 beams have been determined to be 80%, 95% and 99% of the expected respective ultimate capacities. The present analysis confirms the reduced likelihood of IC debonding propagation at lower loads, in particular, within the beams where the tension steel remains elastic [2]. This behaviour differs from the typical case of plate-end debonding where the failure load significantly drops when the plate is curtailed away from the beam support [1].

The analysis of similar four-point bending beams with comparable dimensions (i.e. beam spans in the range of 1000–4500 mm with depths 100–300 mm) gave similar results; a crack 2–3 mm long initiating at a half beam depth away from the loading point towards the support would cause debonding at a load close to the expected ultimate capacity [1].

7.2. Examples: IC debonding initiating by widening of flexural/shear cracks

When no critical interface cracks develop in the highest moment zone, debonding can be caused by a longer flaw initiated at a flexural/shear crack in lower energy zone. This mode of IC debonding has not commonly been observed but can be expected in beams with low span:depth ratios because significant vertical relative sliding between the crack surfaces associated with dominant shear cracks will cause longer interface flaws that may be capable of propagating.

Fig. 13a shows G_R vs. l_d plot for a short beam (B1) (span: depth ratio of 3) tested in [12]. Ten millimeter crushed aggregate was used, so G_{Cl} is assumed to be 0.10 N/mm. Debonding initiated from a flexural/shear crack located about one beam depth (about one third of shear span) offset from the nearest loading point. The figure shows that l_{d_cr} of 5 mm would cause debonding, validating the observation of the formation of much longer interface cracks by widening of flexural/shear cracks. The same figure also shows that a shorter 2 mm crack could have caused debonding at the same load a further half beam depth towards the beam centre, which is the noted critical debonding location for flexure-dominant beams. This is the same magnitude of l_{d_cr} that was needed in the flexure-dominant beams discussed above. In this particular case it appears that a longer flaw emanating from a shear crack occurred before a shorter flaw emanating from a flexural crack. The possibility that debonding initiates at the noted critical location at 90% of $P_{failure}$ is investigated in Fig. 13b (dashed lines in the figure). The figure shows that l_{d_cr} here should be about twice that required at $P_{failure}$.

Once the plate has fully debonded up to the plate end, the propagation of failure towards the opposite direction starting from the original debonding location (Point A in Fig. 14a) is also investigated. The analysis is same as that of PE debonding discussed above since the peeled plate carries no force. The analysis shows that this propagation is possible (Fig. 14b) and is validated by the observation of the separation of a much thicker layer of concrete during debonding in that direction (i.e. starting from Point A and propagates towards the beam centre – Fig. 14a).

Table 2
l_{d_cr} for the Ross et al. (1999) test beams.

Beam	$P_{failure}/P_{ult}$ (%)	l_{d_cr} (mm)				
		Different starting positions at $P_{failure}$ (distance away from the load point)			At different applied loads (debonding initiating at ½h away from the load point	
		½ h	1 h	1½ h	$P_{failure}$	90% $P_{failure}$
Group 1	80	**2**	3.5	6	**2**	4
Group 2	95	**3**	6	12	**3**	7
Group 3	99	**2.5**	9	17	**2.5**	9

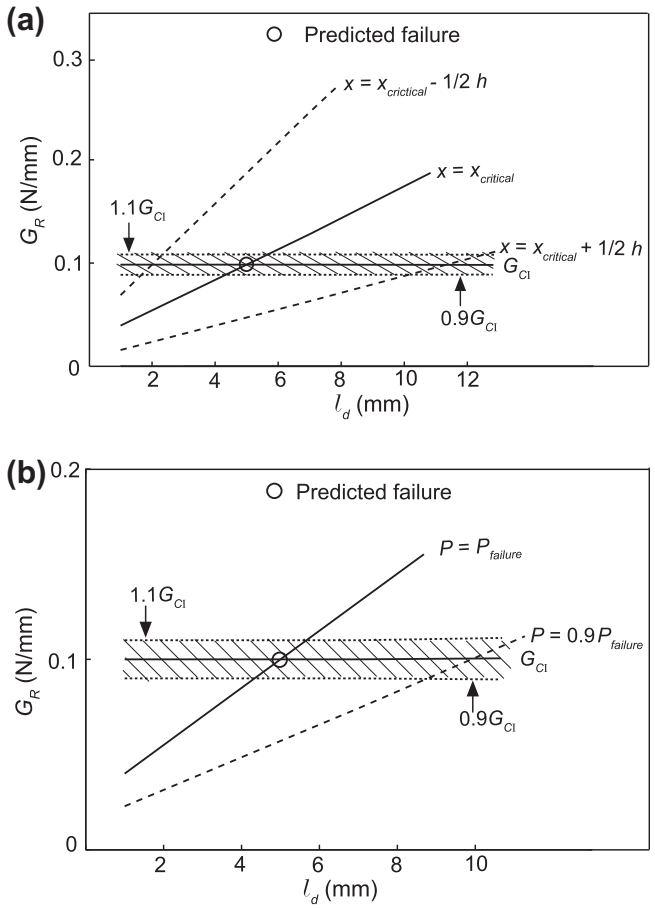

Fig. 13. G_R vs. l_d plot for Beam $3_{U,1.0}$ beam (Garden et al. [12]) for fractures (a) fractures starting at different locations (b) at 90% of the failure load.

8. Discussion

Whilst it is clear that the model can be used to explain why a particular test beam fails, a comprehensive understanding of the likely sizes and locations of interface cracks is required prior to design. There is thus a significant difference between *analysing* the mechanism of failure of a laboratory test and *designing* a structure for use in the real world. This paper explains why it may be impossible ever to predict the exact failure load of beam that is being designed.

8.1. Plate-end debonding

8.1.1. Plate-end debonding initiating in the plate-end vicinity

It has been shown that the calculated G_R and hence the predicted debonding load depends upon the selection of L_{0_eff}, so the length of the interface crack that develops prior to reaching the critical debonding state must therefore be known. It is not trivial to determine whether the critical state will occur prior to the interface crack reaching the internal tension steel or whether additional crack extension at the steel level is required. Most beams have cover depths (c) of 20–30 mm, so a sizeable crack can occur before the internal steel is reached. The present analysis cannot, *a priori*, predict the exact mode. For example, Beam A950 in [10], discussed above, failed due to an infinitesimal interface crack developed at the actual plate end, but it would have also failed at 90% of the reported failure load if there had been a 20 mm long interface crack (Fig. 9a).

8.1.2. Plate-end debonding initiating by widening of shear cracks in the span

It is also not trivial to decide whether an interface crack in the plate-end vicinity or the widening of a shear crack in the span will initiate PE debonding in a given beam, although the latter mode is commonly observed when the external plate extends up to the beam support. The location of the critical shear crack will govern the failure load in this mode, but predicting the precise location of a shear crack is virtually impossible.

The actual failure mechanism may depend upon several factors such as the rate of loading, the exact microstructure of the beam, existing flaw sizes, shear strength of the beam etc.; it is contended that an analysis covering all these features is virtually impossible because such details cannot be known. The present analysis nevertheless accurately predicts the critical location for plate-end-anchoring devices to withstand a required design load (provided that there will be no premature failures of the anchoring devices). The model is also capable of explaining the characteristics of test data.

8.2. Intermediate-crack-induced debonding

It has been shown that in most four-point bending beams, IC debonding is caused by cracks 2–3 mm long initiated due to the widening of flexural cracks at about half beam depth away from the loading point. This agrees with direct test observations (e.g. [12]), despite the influence of various factors such as the surface preparation prior to plate bonding, adhesive type and curing procedure, microstructural features of concrete, etc. on critical crack length being unknown.

IC debonding usually takes place at higher applied loads, very close to the expected ultimate capacity of the strengthened beam. The load range which would cause premature PE debonding is incapable of causing IC debonding, in particular, if the tension steel remains elastic [2].

8.3. Parametric study for design

As presented here, the present model is too complex for use in design. The model could however form the basis of a parametric study that could

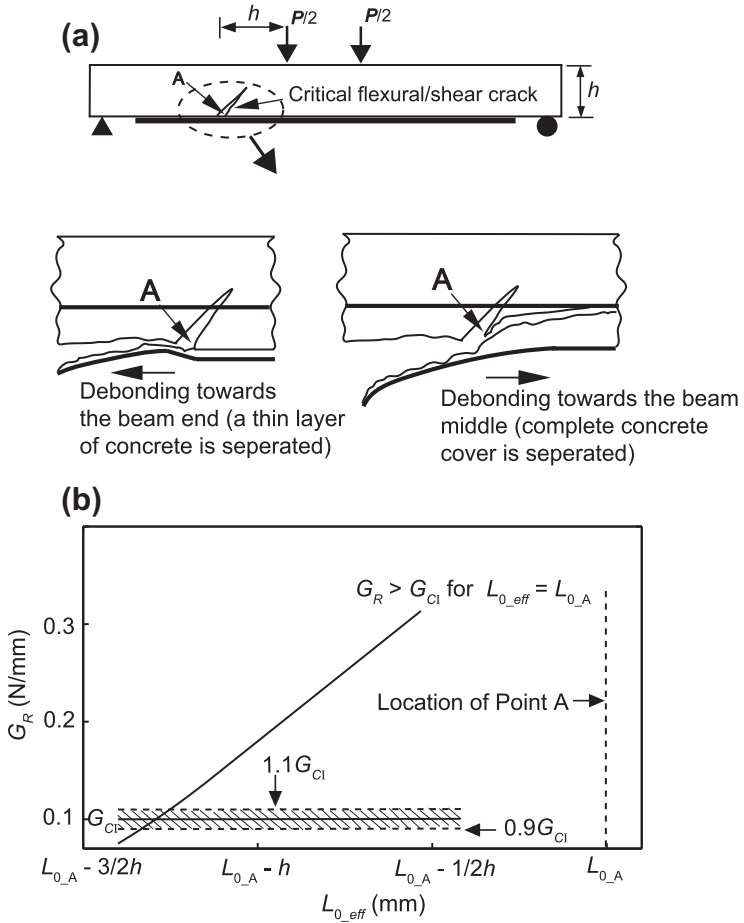

Fig. 14. Complete failure of Beam $3_{U,1.0}$ (a) thick concrete layer is separated during debonding into the beam (b) higher G_R values confirm debonding into the beam.

- identify the parameters that are most important in controlling premature debonding,
- identify how sensitive the debonding load is to changes in those parameters, and
- provide guidance to design as to the approximate values of the parameters that should be used (or perhaps, avoided) when designing beams.

That study is currently in progress.

9. Conclusions

The study has shown that the phenomena of plate debonding can be studied by means of a global-energy-balance based fracture-mechanics approach, which obviates the need for a finite-element analysis of dubious validity. Debonding often propagates in the concrete just above the interface and it has been assumed that extension of debonding is a Mode I propagation as an average, even if the local details may not be Mode I governed; comparisons with test data validate this assumption.

Knowledge of the exact location where the critical debonding initiates is a prerequisite in the analysis of plate-end debonding. It has been found that a location between the actual plate end and a further cover distance into the beam shows accurate predictions for PE debonding in beams with plates curtailed some distance away from the beam support. When the FRP is extended towards the beam support debonding will initiate by either additional, approximately horizontal extension of the original crack at the steel level or from the toe of a shear crack some distance away from the plate end.

Despite exact lengths and locations of the interface flaws being unknowable, it has been shown that justifiable assumptions on *likely* details give comparable predictions with IC debonding test data.

Comparisons with experimental results given above, and others not shown here, demonstrate that the present model is accurate against all forms of plate debonding. It is believed that the basis of the present work could be effectively used in other applications such as the plate debonding analysis of continuous beams and pre-cracked beams, where external strengthening may be most useful.

References

[1] Achintha PMM, Burgoyne CJ. Fracture mechanics of plate debonding. J Compos Constr 2008;12(4):396–404.
[2] Achintha PMM. Fracture analysis of debonding mechanism for FRP plates. PhD Thesis. University of Cambridge, UK; 2009.
[3] Hutchinson JW, Suo Z. Mixed-mode cracking in layered materials. Adv Appl Mech 1992;29:63–191 [In: Hutchinson, JW, TY Wu, editors].
[4] Günes O. A fracture based approach to understanding debonding in FRP bonded structural members. PhD Thesis, Massachusetts Institute of Technology, USA; 2004.
[5] Achintha PMM, Burgoyne CJ. Moment–curvature and strain energy of beams with external FRP reinforcement. ACI Struct J 2009;106(1):20–9.
[6] Achintha PMM, Burgoyne CJ. Fracture energy of the concrete–FRP interface; in preparation.
[7] Bouiadjra BB, Fekirini H, Bouyabout B, Serier B. Fracture energy for repaired cracks with bonded composite patch having two adhesive bands in aircraft structures. Comput Mat Sci 2007;40(1):20–6.
[8] Arduini M, Di Tommaso A, Nanni A. Brittle failure in FRP plate and sheet bonded beams. ACI Struct J 1997;94(4):363–70.

[9] Fanning PJ, Kelly O. Ultimate response of RC beams strengthened with CFRP plates. J Compos Constr 2001;5(2):122–7.
[10] Nguyen DM, Chan TK, Cheong HK. Brittle failure and bond development length of CFRP–concrete beams. J Compos Constr 2001;5(1):12–7.
[11] Mohamed Ali MS, Oehlers DJ, Bradford MA. Shear peeling of steel plates bonded to tension faces of RC beams. J Struct Eng 2001;127(2):1453–9.
[12] Garden HN, Quantrill RJ, Hollaway LC, Thorne AM, Parke GAR. An experimental study of the anchorage length of carbon fibre composite plates used to strengthen reinforced concrete beams. Constr Build Mater 1998;12(4):203–19.
[13] Fracture Mechanics Test Methods for Concrete. RILEM Report 5. In: Shah SP, Carpinteri A, editors. Chapman & Hall; 1991.
[14] Karihaloo BL, Abdalla HM, Imjai T. A simple method for determining the true fracture energies of concrete. Mag Concr Res 2003;55(5):471–81.
[15] Triantafillou T, Plevris N. Strengthening of RC beams with epoxy-bonded fibre reinforced composites. Mater Struct 1992;25(4):201–11.
[16] Quantrill RJ, Hollaway LC, Thorne AM. Experimental and analytical investigation of FRP strengthened beam response: part I. Mag Concr Res 1996;48(4):331–42.
[17] Ross CA, Jerome DM, Tedesco JW, Hughes ML. Strengthening of reinforced concrete beams with externally bonded composite laminates. ACI Struct J 1999;96(2):212–20.